Revisiting Error Analysis in Convolutionally Coded Systems: The Irregular Constellation Case

Mehmet Cagri Ilter, *Student Member, IEEE*, Pawel A. Dmochowski, *Senior Member, IEEE*, and Halim Yanikomeroglu, *Fellow, IEEE*

***Abstract*— There has been a rejuvenated interest in the use of non-equally spaced (irregular) constellations after promising performance results were demonstrated compared with the conventional lattice constellations. This paper investigates the use of the irregular constellations in convolutionally coded systems. To enable the use of such irregular constellations in the presence of convolutional encoders, we derive a bit-error-rate (BER) upper bound expression for the downlink of the coded transmit maximum ratio combining systems operating in Nakagami-*m* fading environments. In addition, the analysis is extended to turbo trellis-coded modulation scenarios in which the convolutional encoders are used as the constituent codes. We demonstrate, via simulation, that commonly used performance analysis techniques in the literature fail to provide a valid BER bound in coded cases where quasi-regularity is not satisfied. In contrast, the technique proposed herein does not require the chosen pair of constellation and encoder to be quasi-regular. Furthermore, the system model includes a provision for multiple orthogonal transmission stages with different numbers of transmit antennas. Antenna correlation as well as distributed transmission is also supported by the model. Simulation results demonstrate the accuracy of the derived analytical results for a wide range of system scenarios.**

***Index Terms*— Convolutional codes, irregular signal constellation, error correction coding, transmit ratio maximum combining, turbo trellis-coded modulation.**

I. Introduction

THE use of convolutional encoders is still prevalent in current and emerging wireless applications, although very powerful codes such as polar and LDPC codes, have become available to reach the channel capacity [1]. Aside from their simplicity, another advantage of using convolutional encoders in current systems is that the aforementioned powerful codes required very large block lengths, and consequently meaning they fail to fulfill the short delay tolerance [2], [3], critical to a number of next-generation applications. Therefore, well-designed convolutionally coded systems can be promising for 5G applications in which low-latency is a key design parameter, such as augmented reality and tactile Internet [4].

Along this line of reasoning, it has already been shown that the use of uniformly spaced constellations can cause suboptimal coded system performance in existing wireless communication standards, e.g., HSPA, IEEE.802.11.$a/g/n$, DVB-T2, etc. [5], [6]. Therefore, the use of irregular constellations, which already gives better performance in many uncoded cases [7], might also appear in the convolutionally coded systems.

To meet the increasing demand on high data rate services in wireless networks, multiple antenna system models have also attracted much attention to overcome the detrimental effects of the propagation environment. The Nakagami-*m* distribution provides an accurate fading model for a range of scenarios, including multi-path scattering effects with different scales of time-delay and reflected waves [8]. Due to the fundamental nature of the BER as a performance metric, numerous results exist for both coded and uncoded systems over the Nakagami-*m* fading model. See [9]–[12], and references therein.

Fundamental to evaluating the BER performance of multiple antenna systems in Nakagami-*m* fading is the distribution of the sum of Gamma random variables (RVs), which dates back to [13], where the authors derive the probability density function (PDF) of the sum of independent but not necessarily identically distributed (i.n.i.d) Gamma RVs in the form of an infinite series. Closed-form results were first developed in [14] where PDF and cumulative distribution function (CDF) expressions were derived for sums of squared Nakagami-*m* RVs with integer fading parameters. The results were expressed as weighted sums of Erlang PDFs and CDFs. More recently, [15] has shown that the PDF of the sum of Gamma RVs can be expressed in terms of the Fox $\bar{H}$-function (for non-integer-valued Nakagami-*m* fading parameters) and the Meijer G-function (for integer-valued Nakagami-*m* fading parameters).

In [16], the authors propose upper bound BER expressions for various receiver combining techniques in coherent trellis-coded modulation systems operating in Rayleigh fading environments. These results were later extended to maximum ratio combining in Nakagami-*m* fading by [17]. However, as we will demonstrate in this paper, the existing techniques

Manuscript received March 10, 2017; revised August 3, 2017; accepted October 1, 2017. Date of publication October 9, 2017; date of current version February 14, 2018. This work is supported in part by Huawei Canada Co., Ltd., and in part by the Ontario Ministry of Economic Development and Innovations Ontario Research Fund - Research Excellence (ORF-RE) program. The associate editor coordinating the review of this paper and approving it for publication was H. Yang. *(Corresponding author: Mehmet Cagri Ilter.)*

M. C. Ilter and H. Yanikomeroglu are with the Department of Systems and Computer Engineering, Carleton University, Ottawa, ON K1S 5B6, Canada (e-mail: ilterm@sce.carleton.ca; halim@sce.carleton.ca).

P. A. Dmochowski are with the School of Engineering and Computer Science, Victoria University of Wellington, Wellington 6012, New Zealand (e-mail: pawel.dmochowski@ecs.vuw.ac.nz).

Color versions of one or more of the figures in this paper are available online at http://ieeexplore.ieee.org.

Digital Object Identifier 10.1109/TCOMM.2017.2761382

for obtaining the BER in coded scenarios are applicable only to quasi-regular (QR) systems, where all performance analysis is independent of transmitted sequences [18]. While facilitating analysis, quasi-regularity is not associated with improved performance [19]. Furthermore, many systems are found to be non-QR, especially when encoders are paired with irregular constellations [20]. This should be emphasized since, with the recent revival of constellation design through optimization techniques [21]–[23], the derivation of error performance expressions for irregular constellations remains largely an open problem in coded systems. In [24], we used the product-state matrix technique [25] in the calculation of the generating function to enable the derivation of error bounds for single antenna coded systems with any signal constellations.

In this paper, the concept of irregular constellations in convolutionally coded systems is considered in a well-rounded system model which includes multiple transmission stages and multiple transmit antennas in each transmission stage, for which the system model in [24] constitutes just a simple special case. Resulting from multiple transmit antenna usage, a proper combining scheme is required. With this in mind, the transmit maximum ratio combining (TMRC) technique [26], [27] was selected to use at the transmitter side during each transmission stage to maximize the received signal to noise ratio (SNR). Using new results for the statistics of the sum of Gamma RVs [15], we develop compact expressions for the generating function in such systems. Furthermore, we consider a very flexible system model, one which allows for an arbitrary number of orthogonal transmission stages where each stage can employ a different number of transmit antennas; where each stage can use different irregular constellations, and have different spatial correlation models, along with arbitrarily chosen Nakagami-m fading parameters; and where each stage can be modelled by co-located or distributed transmit antenna structures.

In the described TMRC system model, the receiver side only performs processing of the received data for decoding, while co-phasing of transmitting symbols and feeding the same information into each distributed antenna in each stage takes place in the transmitter. This asymmetric complexity distribution between the transmitter and the receiver parts is inherent to the Internet of Things (IoT) ecosystem, in which robustness of transmitter units against failure and poor performance is required with increasing network intelligence [28].

In addition to comprehensive analysis given for convolutionally coded cases with the existence of irregular constellations, a proper extension of the given analysis into a more sophisticated coding technique where convolutional encoders are seen as constituent codes has great potential to be used in a wider range of scenarios. To this end, the use of irregular constellation over turbo trellis-coded modulation is also examined and the analysis is validated over Monte Carlo simulations.

The remainder of this paper is organized as follows: In Section II, we present the system model. Error performance analysis, including generating function calculation via the product-state matrix technique and its derivations for both correlated and uncorrelated Nakagami-m fading cases, are given in Section III. Sufficient conditions for quasi-regularity are discussed in Section IV and the extension to the TTCM case is presented in Section V. Numerical results, including the comparison of conventional generating function calculation with the product-state matrix technique and derived BER bound expressions for a wide range of scenarios, are presented in Section VI, where TTCM demonstrations can also be found. Section VII completes the paper with concluding remarks.

II. TMRC Downlink System

We consider a TMRC system consisting of K orthogonal transmission stages, as shown in Fig. 1. Originally proposed in [17], [29], the orthogonal transmission stages offer a flexible representation of complex systems, such as CoMP, HARQ, and relaying. Each transmission stage, k, employs $N^{(k)}$ transmit antennas, and one receive antenna. The channels between the transmit antennas and the receive antenna are modelled by frequency non-selective Nakagami-m slow fading and characterized by an $N^{(k)} \times 1$ vector, $\mathbf{h}_k$. Each entry of $\mathbf{h}_k$, $h_{k,i}$, corresponding to the channel between ith transmit and the receive antenna in the kth orthogonal stage $\left(i \in \{1, \ldots, N^{(k)}\}, k \in \ \{1, \ldots, K\}\right)$, is a complex Nakagami-$m$ random variable with a shaping parameter $m_{k,i}$ and an average fading power $\Omega_{k,i}$. In a distributed antenna transmitter, we assume that antenna elements co-located in a given cluster experience fading governed by a common parameter m_k and fading power Ω_k. We assume independent fading between the K orthogonal transmission stages, with possibly different shaping parameters $m_{k,i}$ and link powers $\Omega_{k,i}$. The envelope of the channel gain, $\left|h_{k,i}\right|$, is modelled by the Nakagami-m distribution with a PDF given by

$$f_{|h_{k,i}|}(h) = \frac{2m_{k,i}^{m_{k,i}} h^{2m_{k,i}-1}}{\Omega_{k,i}\Gamma\left(m_{k,i}\right)} e^{-\frac{m_{k,i}}{\Omega_{k,i}}h}, \tag{1}$$

where $h_{k,i} = |h_{k,i}|e^{-j\theta_{k,i}}$. Note that the Nakagami-m model in the analysis covers the various fading environments from additive white Gaussian noise (AWGN) channel $\left(m_{k,i} \to \infty\right)$ to deep fades $\left(m_{k,i} \to 1/2\right)$ and reduces to a Rayleigh channel for $m_{k,i} = 1$. Within each transmission stage, we consider spatial correlation governed by a matrix $\mathbf{R}_k$. The amount of correlation between co-located antennas i and j, is denoted by the element of $[\mathbf{R}_k]_{i,j} = \rho_{ij}$ and we assume no correlation is present between antennas belonging to different clusters.

In the kth transmission stage, the information symbols are convolutionally encoded and the resulting bits are assigned an output symbol, $s^{(k)}$, based on the specific constellation $\chi^{(k)}$. We assume that perfect channel state information (CSI) is available at the transmitter and the receiver. Each transmitter employs a precoder, $\mathbf{w}_k$, matched to the normalized channel vector $\mathbf{h}_k$,

$$\mathbf{w}_k = \frac{\mathbf{h}_k^H}{\|\mathbf{h}_k\|}, \tag{2}$$

where $\|\cdot\|$ denotes the Euclidean norm. The received signal during the kth transmission stage is given by

$$y_k = \mathbf{h}_k \mathbf{w}_k s^{(k)} + n_k = \alpha_k s^{(k)} + n_k, \tag{3}$$

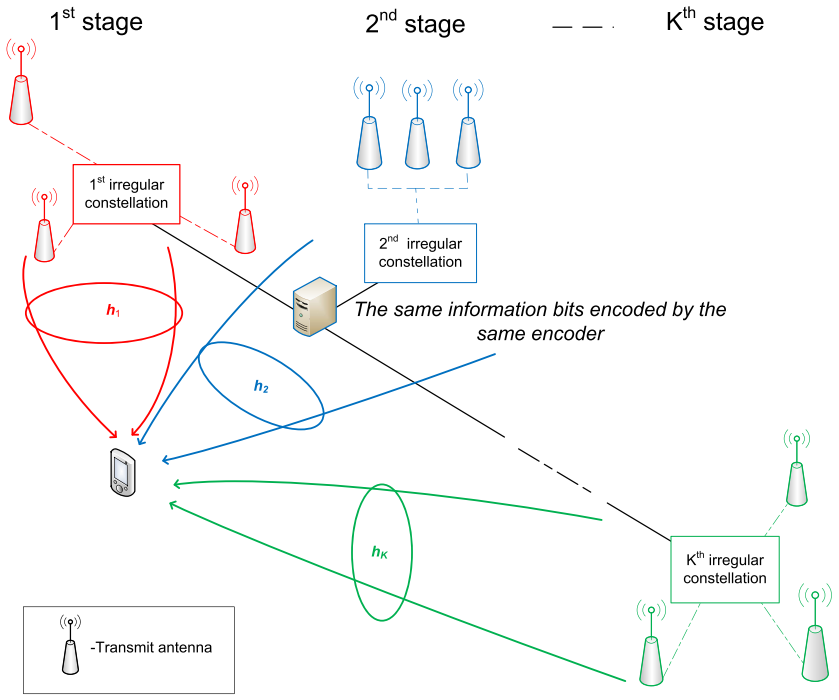

Fig. 1. TMRC with multiple orthogonal transmission stage downlink system model.

where $\alpha_k = \frac{\mathbf{h}_k{}^H \mathbf{h}_k}{\|\mathbf{h}_k\|} = \|\mathbf{h}_k\|$ and n_k is the AWGN sample with zero-mean and $N_0/2$ variance per dimension.

III. Performance Analysis

A. BER Bound Methodology

We begin with an outline of the BER methodology based on the product-state matrix technique [24], [30]. The probability of decoding an erroneous codeword vector $\hat{\mathbf{s}} = [\hat{s}^{(1)}\hat{s}^{(2)}\ldots\hat{s}^{(K)}]$ at the receiver in place of the transmitted codeword $\mathbf{s} = [s^{(1)}s^{(2)}\ldots s^{(K)}]$, where $\exists k, s^{(k)} \neq \hat{s}^{(k)}$ can be expressed in terms of the probability of an erroneous decoder transition $(\upsilon \to \bar{\upsilon})$ for an actual transition state at encoder $(u \to \bar{u})$, which we denote by $D_{(u,\upsilon),(\bar{u},\bar{\upsilon})}$. For a given channel coefficient set, $\mathbf{h}_1, \ldots, \mathbf{h}_K$, the conditional $D_{(u,\upsilon),(\bar{u},\bar{\upsilon})}$ can be expressed as [9]

$$D_{(u,\upsilon),(\bar{u},\bar{\upsilon})|\mathbf{h}_1\ldots\mathbf{h}_K} = \Pr\left(\sum_{k=1}^{K}\left|y_k - \alpha_k s^{(k)}\right|^2 \left|y_k - \alpha_k \hat{s}^{(k)}\right|^2 \geq 0 \,|\mathbf{h}_1 \ldots \mathbf{h}_K\right). \tag{4}$$

After some mathematical manipulations, the Chernoff bound expression for (4) can be written as [9]

$$D_{(u,\upsilon),(\bar{u},\bar{\upsilon})|\mathbf{h}_1,\ldots,\mathbf{h}_K} = e^{-\sum_{k=1}^{K} d_k X_k}, \tag{5}$$

where $d_k = \frac{|s^{(k)} - \hat{s}^{(k)}|^2}{4N_0}$ and $X_k = \alpha_k^2$ is a sum of squared envelope Nakagami-m faded coefficients or, equivalently, the sum of Gamma variables. The unconditional $D_{(u,\upsilon),(\bar{u},\bar{\upsilon})}$ can be calculated using

$$D_{(u,\upsilon),(\bar{u},\bar{\upsilon})} = \prod_{k=1}^{K}\int_0^{\infty} e^{-d_k X_k} f_{X_k}(X_k)\, dX_k, \tag{6}$$

TABLE I
Classification of the Product-States.

$\mathbf{S}$	$u = \upsilon$	$u \neq \upsilon$
$\bar{u} = \bar{\upsilon}$	$S_{\mathcal{GG}}$	$S_{\mathcal{BG}}$
$\bar{u} \neq \bar{\upsilon}$	$S_{\mathcal{GB}}$	$S_{\mathcal{BB}}$

where $f_{X_k}(X_k)$ denotes the PDF of X_k.

In order to evaluate the error performance of the TMRC downlink system, the generating function of the encoder needs to be computed. The generating function, $T(I)$, includes all possible squared distances between transmitted and decoded symbols. Before constructing the product-state matrix, $\mathbf{S}$, the definition of 'good' $(\mathcal{G})$ and 'bad' $(\mathcal{B})$ states should be given. The classification of a given pair state is determined by a simple rule based on comparing initial and final states of possible pairs of transitions [30] as shown in Table I, where $u \to \bar{u}$ and $\upsilon \to \bar{\upsilon}$ denote the state transition at the encoder and decoder, respectively.

Using this classification and suitably ordering the product-states, $\mathbf{S}$ can be written in the form of [25]

$$\mathbf{S} = \begin{bmatrix} \mathbf{S}_{\mathcal{GG}} & \mathbf{S}_{\mathcal{GB}} \\ \mathbf{S}_{\mathcal{BG}} & \mathbf{S}_{\mathcal{BB}} \end{bmatrix}. \tag{7}$$

A particular entry of $\mathbf{S}$, $\mathbf{S}_{(u,\upsilon),(\bar{u},\bar{\upsilon})}$, can be expressed by

$$\mathbf{S}_{(u,\upsilon),(\bar{u},\bar{\upsilon})} = \Pr(u \to \bar{u}|u) \times \sum_n p_n I^{\mathrm{W}(u\to\bar{u})\oplus\mathrm{W}(\upsilon\to\bar{\upsilon})} D_{(u,\upsilon),(\bar{u},\bar{\upsilon})}, \tag{8}$$

where the summation in (8) is over all possible n parallel transitions depending on a given encoder, p_n denotes the probability of the nth parallel transition between $(u \to \bar{u})$ if it exists, otherwise $p_n = 1$. $\Pr(u \to \bar{u}|u)$ is the conditional

probability of a transition from state u to state $\bar{u}$, given state u and $\mathrm{W}(i \to j)$ denotes the Hamming weight of the information sequence for the transition from i to j where $i \in \{u, \upsilon\}$ and $j \in \{\bar{u}, \bar{\upsilon}\}$ [30].

After obtaining each entry of $\mathbf{S}$, the generating function, $T(I)$, can be computed by [25]

$$T(I) = \mathbf{1}^T \mathbf{S}_{\mathcal{G}\mathcal{G}} \mathbf{1} + \left(\mathbf{1}^T \mathbf{S}_{\mathcal{G}\mathcal{B}}\right)^T \left[\mathbf{I} - \mathbf{S}_{\mathcal{B}\mathcal{B}}\right]^{-1} \mathbf{S}_{\mathcal{B}\mathcal{G}} \mathbf{1}, \tag{9}$$

where $\mathbf{1}$ and $\mathbf{I}$ denote the unity and identity matrices, respectively. Using (9), one can compute the upper bound BER [31]

$$P_b \leq \frac{1}{l} \frac{\partial T(I)}{\partial I}\bigg|_{I=1}, \tag{10}$$

where l denotes the number of information bits per output symbol. The derivative of (10) can be easily shown to be [25]

$$\begin{aligned}\frac{\partial T(I)}{\partial I} &= \frac{1}{2N}\Big(\left(\mathbf{1}^T \mathbf{S}_{\mathcal{G}\mathcal{G}}(I)\right)' + \left(\mathbf{1}^T \mathbf{S}_{\mathcal{G}\mathcal{B}}(I)\right)'^T \left[\mathbf{I} - \mathbf{S}_{\mathcal{B}\mathcal{B}}(I)\right]^{-1} \\ &\quad \times \mathbf{S}_{\mathcal{B}\mathcal{G}}(I)\,\mathbf{1} + \left(\mathbf{1}^T \mathbf{S}_{\mathcal{G}\mathcal{B}}(I)\right)^T \left[\mathbf{I} - \mathbf{S}_{\mathcal{B}\mathcal{B}}(I)\right]^{-1} \left(\mathbf{S}_{\mathcal{B}\mathcal{G}}(D, I)\,\mathbf{1}\right)' \\ &\quad + \left(\mathbf{1}^T \mathbf{S}_{\mathcal{G}\mathcal{B}}(I)\right)^T \left[\mathbf{I} - \mathbf{S}_{\mathcal{B}\mathcal{B}}(I)\right]^{-1} \mathbf{S}_{\mathcal{B}\mathcal{B}}(I)' \left[\mathbf{I} - \mathbf{S}_{\mathcal{B}\mathcal{B}}(I)\right]^{-1} \\ &\quad \times \mathbf{S}_{\mathcal{B}\mathcal{G}}(I)\,\mathbf{1}\Big),\end{aligned} \tag{11}$$

where $(\cdot)'$ denotes element-wise derivative with respect to I.

We now proceed to derive the unconditional $D_{(u,\upsilon),(\bar{u},\bar{\upsilon})}$ for a number of fading scenarios. The resulting expressions are then used in (8)-(10) to obtain the BER bound.

B. $D_{(u,\upsilon),(\bar{u},\bar{\upsilon})}$ for General m-Parameters

We begin with the closed-form expression for the PDF of X_k for non-integer fading parameters, which can be written in terms of Fox's $\bar{H}$-function which is obtained from the product of moment generating functions (MGF) of $|h_{k,i}|^2$'s [15], as

$$f_{X_k}(X_k) = \prod_{i=1}^{N^{(k)}} \left(\frac{m_{k,i}}{\Omega_{k,i}}\right)^{m_{k,i}} \bar{\mathrm{H}}^{0,N^{(k)}}_{N^{(k)},N^{(k)}} \left[e^{X_k} \,\middle|\, \begin{matrix} \Xi^{(1)}_{N^{(k)}} \\ \Xi^{(2)}_{N^{(k)}} \end{matrix} \right], \tag{12}$$

where the explicit definition of Fox's $\bar{H}$-function can be found in Table II. The coefficient sets $\Xi^{(1)}_{N^{(k)}}$ and $\Xi^{(2)}_{N^{(k)}}$ are defined as [15]

$$\begin{aligned}\Xi^{(1)}_{N^{(k)}} &= \overbrace{\left(1 - \frac{m_{k,1}}{\Omega_{k,1}}, 1, m_{k,1}\right), \cdots, \left(1 - \frac{m_{k,N^{(k)}}}{\Omega_{k,N^{(k)}}}, 1, m_{k,N^{(k)}}\right)}^{N^{(k)}-\text{bracketed terms}}, \\ \Xi^{(2)}_{N^{(k)}} &= \overbrace{\left(-\frac{m_{k,1}}{\Omega_{k,1}}, 1, m_{k,1}\right), \cdots, \left(-\frac{m_{k,N^{(k)}}}{\Omega_{k,N^{(k)}}}, 1, m_{k,N^{(k)}}\right)}^{N^{(k)}-\text{bracketed terms}}.\end{aligned} \tag{13}$$

Substituting (12) into (6) gives

$$D_{(u,\upsilon),(\bar{u},\bar{\upsilon})} = \prod_{k=1}^{K} \prod_{i=1}^{N^{(k)}} \left(\frac{m_{k,i}}{\Omega_{k,i}}\right)^{m_{k,i}} Z_k, \tag{14}$$

where Z_k is defined by

$$Z_k = \int_0^\infty e^{-d_k X_k} \bar{\mathrm{H}}^{0,N^{(k)}}_{N^{(k)},N^{(k)}} \left[e^{X_k} \,\middle|\, \begin{matrix} \Xi^{(1)}_{N^{(k)}} \\ \Xi^{(2)}_{N^{(k)}} \end{matrix} \right] dX_k. \tag{15}$$

Using the explicit definition of Fox's $\bar{H}$-function given above, (15) can be rewritten in the form of a Mellin-Barnes contour integral [15],

$$Z_k = \int_0^\infty e^{-d_k X_k} \frac{1}{2\pi i} \oint_C \frac{\prod_{j=1}^{N^{(k)}} \Gamma\left(1 - \alpha_j + A_j\right)^{a_j}}{\prod_{j=1}^{N^{(k)}} \Gamma\left(1 - \beta_j + B_j\right)^{b_j}} e^{s X_k} ds\, dX_k. \tag{16}$$

Here, (α_j, A_j, a_j) and (β_j, B_j, b_j) correspond to the elements of the jth coefficient in (13). Utilizing the Gamma function definition [32, 8.331.1], we obtain the following expression for the first integral in (16)

$$\int_0^\infty e^{-d_k X_k} e^{s X_k} dX_k = \frac{1}{d_k - s} = -\frac{\Gamma(s - d_k)}{\Gamma(s - d_k + 1)}. \tag{17}$$

Interchanging the order of integrals in (16) and using (17) and [15, (A.2)], Z_k can be expressed as

$$\begin{aligned} l Z_k &= -\oint_C \frac{\prod_{j=1}^{N^{(k)}} \Gamma\left(1 - \alpha_j + A_j\right)^{a_j}}{\prod_{j=1}^{N^{(k)}} \Gamma\left(1 - \beta_j + B_j\right)^{b_j}} \frac{\Gamma(s - d_k)}{\Gamma(s - d_k + 1)} ds \\ &= -\bar{\mathrm{H}}^{0,N^{(k)}+1}_{N^{(k)}+1,N^{(k)}+1} \left[1 \,\middle|\, \begin{matrix} \Xi^{(1)}_{N^{(k)}}, (1 + d_k, 1, 1) \\ \Xi^{(2)}_{N^{(k)}}, (d_k, 1, 1) \end{matrix} \right], \end{aligned} \tag{18}$$

giving the result for $D_{(u,\upsilon),(\bar{u},\bar{\upsilon})}$ of

$$\begin{aligned} D_{(u,\upsilon),(\bar{u},\bar{\upsilon})} = \prod_{k=1}^{K} \prod_{i=1}^{N^{(k)}} -\left(\frac{m_{k,i}}{\Omega_{k,i}}\right)^{m_{k,i}} &\times \bar{\mathrm{H}}^{0,N^{(k)}+1}_{N^{(k)}+1,N^{(k)}+1} \\ &\times \left[1 \,\middle|\, \begin{matrix} \Xi^{(1)}_{N^{(k)}}, (1+d_k, 1, 1) \\ \Xi^{(2)}_{N^{(k)}}, (d_k, 1, 1) \end{matrix} \right]. \end{aligned} \tag{19}$$

C. $D_{(u,\upsilon),(\bar{u},\bar{\upsilon})}$ for Integer m-Parameters

While (12) gives the distribution characteristics of X_k for any value of $m_{k,i}$, it includes the Fox's $\bar{H}$ function which currently has limited availability in the standard mathematical packages. Considering integer-valued m-parameters for Nakagami-m fading channels significantly simplifies the analysis, whereby the results can be expressed as fractional products.

In the case of integer-valued $m_{k,i}$, (12) simplifies to a closed-form PDF expression given by [33]

$$f_{X_k}(X_k) = \prod_{i=1}^{N^{(k)}} \left(\frac{m_{k,i}}{\Omega_{k,i}}\right)^{m_{k,i}} G^{\kappa,0}_{\kappa,\kappa} \left(e^{-X_k} \,\middle|\, \begin{matrix} \psi^{(1)}_\kappa \\ \psi^{(2)}_\kappa \end{matrix} \right), \tag{20}$$

TABLE II
DEFINITION OF THE FOX'S $\bar{\text{H}}$ AND MEIJER'S G-FUNCTIONS

The definition of Fox's $\bar{\text{H}}$-function results from the following contour integral, which is given as [15]

$$\bar{\text{H}}_{p,q}^{m,n}\left[z| \begin{matrix}(\alpha_j, A_j, a_j)_{1,n}, (\alpha_j, A_j)_{n+1,p} \\ (\beta_j, B_j)_{1,m}, (\beta_j, B_j, b_j)_{m+1,q}\end{matrix}\right] = \frac{1}{2\pi i}\oint_C \frac{\prod_{j=1}^{n}\{\Gamma(1-\alpha_j+A_j s)\}^{a_j}\prod_{j=1}^{m}\Gamma(\beta_j - B_j s)}{\prod_{j=n+1}^{p}\Gamma(\alpha_j - A_j s)\prod_{j=m+1}^{q}\{\Gamma(1-\beta_j+B_j s)\}^{b_j}} z^s ds,$$

where $\Gamma(\cdot)$ denotes the gamma function [32]. Herein, z can take real or complex values except $z=0$ and the following inequalities are required to be satisfied: $1 \le m \le q,\ 0 \le n \le p, A_j > 0$ for $j = 1, \cdots, p, B_j > 0$ for $j = 1, \cdots, q, \alpha_j, \beta_j \in \mathbb{C}, a_j, b_j \notin \mathbb{Z}$.

As a special case of the Fox's $\bar{\text{H}}$-function, where $A_j = B_j = 1$ and $a_j = b_j = 1$ for all j, Meijer G-function is defined as [32]

$$\text{G}_{p,q}^{m,n}\left[z| \begin{matrix}(\alpha_1, \cdots, \alpha_p) \\ (\beta_1, \cdots, \beta_q)\end{matrix}\right] = \frac{1}{2\pi i}\oint_C \frac{\prod_{j=1}^{n}\Gamma(1-\alpha_j+s)\prod_{j=1}^{m}\Gamma(\beta_j - s)}{\prod_{j=n+1}^{p}\Gamma(\alpha_j - s)\prod_{j=m+1}^{q}\Gamma(1-\beta_j+s)} z^s ds.$$

where $\Gamma(\cdot)$ denotes the gamma function [32]. Herein, z can take real or complex values except $z=0$ and the following inequalities are required to be satisfied: $1 \le m \le q,\ 0 \le n \le p,\ \alpha_j, \beta_j \in \mathbb{C}, a_j, b_j \notin \mathbb{Z}$.

where $G_{p,q}^{m,n}\left(x \left| \begin{matrix}\psi_\kappa^{(1)} \\ \psi_\kappa^{(2)}\end{matrix}\right.\right)$ denotes the Meijer G-function where its explicit definition can be also found in Table II, $\kappa = \sum_{i=1}^{N^{(k)}} m_{k,i}$ is an integer, and the coefficient sets $\psi_\kappa^{(1)}$ and $\psi_\kappa^{(2)}$ are defined as [33]

$$\psi_\kappa^{(1)} = \overbrace{\underbrace{\left(1+\frac{m_{k,1}}{\Omega_{k,1}}\right),\cdots,}_{m_{k,1}-\text{times}},\ldots,\underbrace{\left(1+\frac{m_{k,N^{(k)}}}{\Omega_{k,N^{(k)}}}\right),\cdots,}_{m_{k,N^{(k)}}-\text{times}}}^{\kappa-\text{bracketed terms}}$$

$$\psi_\kappa^{(2)} = \overbrace{\underbrace{\left(\frac{m_{k,1}}{\Omega_{k,1}}\right),\cdots,}_{m_{k,1}-\text{times}},\ldots,\underbrace{\left(\frac{m_{k,N^{(k)}}}{\Omega_{k,N^{(k)}}}\right),\cdots.}_{m_{k,N^{(k)}}-\text{times}}}^{\kappa-\text{bracketed terms}} \tag{21}$$

Averaging (5) over the PDFs of X_k in (20), $D_{(u,v),(\bar{u},\bar{v})}$ can be expressed by

$$D_{(u,v),(\bar{u},\bar{v})} = \prod_{k=1}^{K}\prod_{i=1}^{N^{(k)}}\left(\frac{m_{k,i}}{\Omega_{k,i}}\right)^{m_{k,i}} Z_k, \tag{22}$$

where Z_k is given by

$$Z_k = \int_0^\infty e^{-d_k X_k} G_{\kappa,\kappa}^{\kappa,0}\left(e^{-X_k}\left|\begin{matrix}\psi_\kappa^{(1)} \\ \psi_\kappa^{(2)}\end{matrix}\right.\right) dX_k\ . \tag{23}$$

The closed-from solution of (23), along with intermediate steps, is given in Appendix A. Using that result, the final expression for $D_{(u,v),(\bar{u},\bar{v})}$ can be obtained as

$$D_{(u,v),(\bar{u},\bar{v})} = \prod_{k=1}^{K}\prod_{i=1}^{N^{(k)}}\left(1+d_k\frac{\Omega_{k,i}}{m_{k,i}}\right)^{-m_{k,i}}. \tag{24}$$

Simplifying (24) for $N^{(1)} = 1, K = 1$ reduces to a single-input single-output (SISO) case derived in [24].[1]

[1]Note that [24, (9)] contains a typographical error, where the second Ω in each factor should be replaced by "1".

D. $D_{(u,v),(\bar{u},\bar{v})}$ for General m With Correlated Antennas

We now consider a case where spatial correlation exists between the co-located transmit antenna elements. Considering transmit antennas deployed in a cluster, we take $\Omega_k = \Omega_{k,i}$ and $m_k = m_{k,i},\ \forall i$. Here, the MGF of X_k is given by [15]

$$\mathcal{M}_{X_k}(s) = \prod_{i=1}^{N^{(k)}}\left(1 - s\lambda_{k,i}\right)^{m_k}, \tag{25}$$

where $\left\{\lambda_{k,i}\right\}_i^{N^{(k)}}$ are the eigenvalues of the matrix governing the correlation between the channel powers for the antenna elements. We denote this matrix by $\mathbf{A}_k$, where $\mathbf{A}_k = \mathbf{D}_k\mathbf{C}_k$ where $\mathbf{C}_k$ is a $N^{(k)} \times N^{(k)}$ symmetric positive definite matrix and $\mathbf{D}_k$ is a $N^{(k)} \times N^{(k)}$ diagonal matrix with entries Ω_k/m_k, which are given by [34]

$$\mathbf{C}_k = \begin{bmatrix} 1 & \sqrt{\nu_{12}} & \cdots & \sqrt{\nu_{1N^{(k)}}} \\ \sqrt{\nu_{21}} & 1 & & \sqrt{\nu_{2N^{(k)}}} \\ \vdots & & \ddots & \vdots \\ \sqrt{\nu_{N^{(k)}1}} & \cdots & \cdots & 1 \end{bmatrix}, \tag{26}$$

and

$$\mathbf{D}_k = \begin{bmatrix} \Omega_k/m_k & 0 & \cdots & 0 \\ 0 & \Omega_k/m_k & & 0 \\ \vdots & & \ddots & \vdots \\ 0 & \cdots & \cdots & \Omega_k/m_k \end{bmatrix}. \tag{27}$$

Note that the following analysis is clearly applicable to any spatial correlation model since the calculations are independent of how ρ_{ij} is obtained. It should be noted that, the correlation coefficients ν_{ij} in (26) correspond to correlation between powers, $|h_{k,i}|^2$ and $|h_{k,j}|^2$, while ρ_{ij} governs the correlation between the envelopes, $\left|\text{h}_{k,i}\right|$ and $\left|\text{h}_{k,j}\right|$. Their relation is given by [35]

$$\rho_{ij} = \varphi(i,j)\left\{{}_2F_1\left(-\frac{1}{2},-\frac{1}{2};m_k;\nu_{ij}\right) - 1\right\}, \tag{28}$$

and

$$\varphi(i,j) = \frac{\Gamma^2\left(i+\frac{j}{2}\right)}{\Gamma(i)\Gamma(i+j) - \Gamma^2\left(i+\frac{j}{2}\right)}. \tag{29}$$

Herein, $\Gamma(\cdot)$ is the Gamma function and ${}_2F_1(\cdot,\cdot;\cdot;\cdot)$ denotes the Gauss hypergeometric function [32]. In order to solve (28) numerically for any given correlation model, the Newton-Raphson method can be used [35]. The PDF of X_k can be found via the inverse Laplace transform of (25) [15] and is given for non-integer m_k values by [36]

$$f_{X_k}(X_k) = \prod_{i=1}^{N^{(k)}} \left(\frac{1}{\lambda_{k,i}}\right)^{m_k} \bar{\mathrm{H}}^{0,N^{(k)}}_{N^{(k)},N^{(k)}} \left[e^{X_k} \,\middle|\, \begin{matrix} \Xi^{(1)}_{N^{(k)}} \\ \Xi^{(2)}_{N^{(k)}} \end{matrix} \right], \quad (30)$$

where the coefficient sets $\Xi^{(1)}_{N^{(k)}}$ and $\Xi^{(2)}_{N^{(k)}}$ are defined as [36]

$$\Xi^{(1)}_{N^{(k)}} = \overbrace{\left(1-\frac{1}{\lambda_{k,1}},1,m_k\right),\cdots,\left(1-\frac{1}{\lambda_{k,N^{(k)}}},1,m_k\right)}^{N^{(k)}-\text{bracketed terms}},$$
$$\Xi^{(2)}_{N^{(k)}} = \overbrace{\left(-\frac{1}{\lambda_{k,1}},1,m_k\right),\cdots,\left(-\frac{1}{\lambda_{k,N^{(k)}}},1,m_k\right)}^{N^{(k)}-\text{bracketed terms}}. \quad (31)$$

Using (17) and [15, (A.2)], $D_{(u,v),(\bar{u},\bar{v})}$ for non-integer m_k values can be expressed as

$$D_{(u,v),(\bar{u},\bar{v})} = \prod_{k=1}^{K}\prod_{i=1}^{N^{(k)}} \left(\frac{1}{\lambda_{k,i}}\right)^{m_k} Z_k, \quad (32)$$

where Z_k is given as

$$Z_k = -\mathrm{H}^{0,N^{(k)}+1}_{N^{(k)}+1,N^{(k)}+1} \left[1 \,\middle|\, \begin{matrix} \Xi^{(1)}_{N^{(k)}}, (1+d_k,1,1) \\ \Xi^{(2)}_{N^{(k)}}, (d_k,1,1) \end{matrix} \right]. \quad (33)$$

E. $D_{(u,v),(\bar{u},\bar{v})}$ for Integer m With Correlated Antenna

For integer m_k, (20) can be modified to include correlation using the same approach as in Section III-D. The resulting PDF is given by

$$f_{X_k}(X_k) = \prod_{i=1}^{N^{(k)}} \left(\frac{1}{\lambda_{k,i}}\right)^{m_k} G^{\kappa,0}_{\kappa,\kappa}\left(e^{-X_k} \,\middle|\, \begin{matrix} \psi^{(1)}_\kappa \\ \psi^{(2)}_\kappa \end{matrix} \right), \quad (34)$$

where

$$\psi^{(1)}_\kappa = \overbrace{\overbrace{\left(1+\frac{1}{\lambda_{k,1}}\right)}^{m_k-\text{times}},\ldots,\overbrace{\left(1+\frac{1}{\lambda_{k,N^{(k)}}}\right)}^{m_k-\text{times}}}^{N^{(k)}m_k-\text{bracketed terms}}$$
$$\psi^{(2)}_\kappa = \overbrace{\overbrace{\left(\frac{1}{\lambda_{k,1}}\right)}^{m_k-\text{times}},\ldots,\overbrace{\left(\frac{1}{\lambda_{k,N^{(k)}}}\right)}^{m_k-\text{times}}}^{N^{(k)}m_k-\text{bracketed terms}}. \quad (35)$$

$D_{(u,v),(\bar{u},\bar{v})}$ for integer m_k values can be expressed as

$$D_{(u,v),(\bar{u},\bar{v})} = \prod_{k=1}^{K}\prod_{i=1}^{N^{(k)}} \left(\frac{1}{\lambda_{k,i}}\right)^{m_k} Z_k, \quad (36)$$

where

$$Z_k = \left(d_k + \frac{1}{\lambda_{k,i}}\right)^{-m_k}. \quad (37)$$

IV. Quasi-Regularity

At this stage, the quasi-regularity property is discussed to give insight on the necessity of analytical framework in previous section. We demonstrate that not only quasi-regularity is violated with a combination of irregular constellation and convolutional encoder, but also for some conventional constellations. The quasi-regularity property of encoder-constellation pair determines the calculation method of the generating function and a quasi-regular scenario allows a simplified generating function calculation. The two conditions of quasi-regularity for any given encoder and constellation pair are as follows [18]:

- The encoder needs to be linear.
- For all possible error vectors $\mathbf{e}$ and all pairs of states (u,v) and $(\bar{u},\bar{v})$, the following conditions are required to satisfy for each pair of states and each possible error codeword:

$$P_{(u,v),\mathbf{e}}(D) = P_{(\bar{u},\bar{v}),\mathbf{e}}(D). \quad (38)$$

Herein, $P_{(u,v),\mathbf{e}}(D)$ denotes the distance polynomial which is explicitly given by

$$P_{(u,v),\mathbf{e}}(D) = \sum_{\mathbf{c}|u} p(\mathbf{c}|u)\, D^{d^2[g(\mathbf{c}),g(\mathbf{c}\oplus\mathbf{e}))]}, \quad (39)$$

where $p(\mathbf{c}|u)$ is the probability that the vector $\mathbf{c}$ labels a transition emerging from state u to state v, and $d^2[g(\mathbf{c}), g(\mathbf{c}\oplus\mathbf{e})]$ is Euclidean distance between the symbols $g(\mathbf{c})$, resulting from $u \to v$, and $g(\mathbf{c}\oplus\mathbf{e})$ resulting from $\bar{u} \to \bar{v}$. Quasi-regularity is achieved if the coded system satisfies the above two conditions and the conventional generating function calculation can be used to obtain the error performance expression.

In cases of puncturing and erasure, quasi-regularity conditions cannot be satisfied [37]. In some cases, this can be observed with conventional M-QAM and M-PSK constellations. As an example, the rate-1/3 convolutional encoder specified LTE standard used in the downlink control information [38] is not quasi-regular with a 64-QAM constellation.

Quasi-regularity brings simplified error performance calculation; however, it does not imply better or worse performance. While the conventional generating function calculation can be applied in this case, this method fails to give a proper performance metric for non-quasi-regular cases. For this reason, the product-state matrix method [25] was introduced in Section III.

The following example demonstrates that quasi-regularity depends on both the signal constellation and the encoder used. Initially, two arbitrarily generated 4-ary irregular constellations (Constellation-I and Constellation-II), are presented in Fig. 2. Constellation-I and Constellation-II symbol points are $\{-2.17+0.14\mathrm{i}, 0.66-0.84\mathrm{i}, -0.06+0.29\mathrm{i}, -0.62-0.13\mathrm{i}\}$ and $\{1.06+2.64i, -1.72-1.03i, -0.34-0.59i, 1.34+0.72i\}$, respectively. The combination of the $[2,1]_8$ convolutional encoder with Constellation-I violates the quasi-regularity property while the same encoder with Constellation-II satisfies it. The error vector $(\mathbf{1},\mathbf{0})$ violates (39) for the $(u,v)=(0,0)$ and $(\bar{u},\bar{v})=(1,1)$ by yielding two different exponents of D

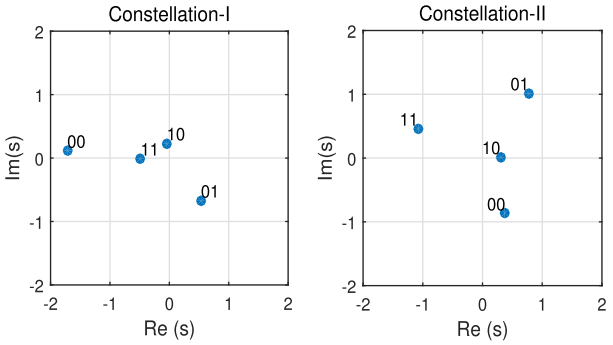

Fig. 2. Constellation-I and Constellation-II.

such that

$$P_{0,0,(\mathbf{1},\mathbf{0})}(D) = D^{d^2[g(\mathbf{00}),g(\mathbf{00}\oplus\mathbf{10}))]} = D^{d^2[g(\mathbf{00}),g(\mathbf{10})]},$$
$$P_{1,1,(\mathbf{1},\mathbf{0})}(D) = D^{d^2[g(\mathbf{01}),g(\mathbf{01}\oplus\mathbf{10}))]} = D^{d^2[g(\mathbf{01}),g(\mathbf{11})]}, \quad (40)$$

which violates (38) with $P_{0,0,(\mathbf{1},\mathbf{0})}(D) \neq P_{1,1,(\mathbf{1},\mathbf{0})}(D)$. The comparison of the conventional generating function calculation with the one calculated from the product-state matrix technique is presented in Section VI, where the different behavior of conventional generating function method based on a choice of constellation can be observed.

V. Extension to Turbo Trellis-Coded Modulation

The potential performance gain resulting from non-uniform constellation usage in coded scenarios [5], [6] provides motivation for the extension of the given framework to more powerful coded techniques. TTCM encoders emerged as an attractive coding technique which combines the powerful design of binary turbo coding [39] with larger constellation sizes [40]. Here, information bits are fed into two convolutional encoders in the same way as binary turbo codes in the TTCM encoder, where a bit-interleaver and a symbol-based interleaver are employed before and after the second encoder, respectively. Output symbols from the first encoder, $\mathbf{s}^{(1)}$, are selected from a M-ary constellation while the interleaved version of original information bits are assigned into the output symbols, $\mathbf{s}^{(2)}$ [40], [41]. After generating M-ary symbols from both the first TCM and the second TCM encoders, $\mathbf{s}^{(1)}$ and $\mathbf{s}^{(2)}$, the output symbols of TTCM-encoded symbols, $\mathbf{s}$, can be selected as follows

$$\mathbf{s} = \left[s_1^{(1)} s_2^{(2)} s_3^{(1)} s_4^{(2)} s_5^{(1)} s_6^{(2)} \dots\right], \quad (41)$$

where $s_t^{(i)}$ denotes an output symbol chosen from the ith TCM encoder at the time instant t $(i \in \{1,2\}, t \geq 0)$ as shown in Fig. 3, $\mathbf{s}^{(1)} = \left[s_1^{(1)} s_2^{(1)} s_3^{(1)} s_4^{(1)} \cdots\right]$, and $\mathbf{s}^{(2)} = \left[s_1^{(2)} s_2^{(2)} s_3^{(2)} s_4^{(2)} \dots\right]$.

A typical error performance of turbo coded systems tends to fall into two categories which are referred to as the "waterfall region" and "error floor region" [39]. As the performance criteria inside the waterfall region is based on EXIT chart analysis [42], the error performance analysis which considers the irregular constellation for TTCM cases is given only for the error floor region. In connection with the process of obtaining a generating function in convolutionally coded cases, the concept of a hyper-trellis, a pair of product-states of each encoder, was introduced in [43], which combines the analysis of two encoders. Following the approach taken for the analysis of quasi-regular cases in [41], each entry of the product-state matrix for the TTCM encoder can be written as

$$\mathbf{S}_{(u_1,u_2,v_1,v_2),(\bar{u}_1,\bar{u}_2,\bar{v}_1,\bar{v}_2)} = \Pr(u_1 \to \bar{u}_1 | u_1)\, I^{\mathcal{W}(u_1\to\bar{u}_1 \oplus v_1\to\bar{v}_1)} \times D_{(u_1,u_2,v_1,v_2),(\bar{u}_1,\bar{u}_2,\bar{v}_1,\bar{v}_2)}, \quad (42)$$

where

$$D_{(u_1,u_2,v_1,v_2),(\bar{u}_1,\bar{u}_2,\bar{v}_1,\bar{v}_2)} = D_{(u_1,v_1),(\bar{u}_1,\bar{v}_1)} D_{(u_2,v_2),(\bar{u}_2,\bar{v}_2)} P_\Pi^N. \quad (43)$$

Here, $\mathbf{S}_{(u_1,u_2,v_1,v_2),(\bar{u}_1,\bar{u}_2,\bar{v}_1,\bar{v}_2)}$ is a hyper-trellis version of two product states, $\mathbf{S}_{(u_1,v_1),(\bar{u}_1,\bar{v}_1)}$ and $\mathbf{S}_{(u_2,v_2),(\bar{u}_2,\bar{v}_2)}$, already given in (8). Here, P_Π^N accounts for the interleaver effect used in the encoder and is related to the number of possible error events having w_o Hamming weight in odd-indices and w_e for even indices with the existence of N information bits, where l is the number of information bits per symbol. In order to take the next step in the analysis, it is assumed that the interleavers used in the encoder are uniform, as in [43]. Then, the explicit definition of P_Π^N can be given by [44]

$$P_\Pi^N = \frac{1}{\binom{N/2}{w_{o,1}}\binom{N/2-w_{o,1}}{w_{o,2}}\cdots\binom{N/2-w_{o,l-1}}{w_{o,l}}} \times \frac{1}{\binom{N/2}{w_{e,1}}\binom{N/2-w_{e,1}}{w_{e,2}}\cdots\binom{N/2-w_{e,l-1}}{w_{e,l}}}. \quad (44)$$

Once $D_{(u_1,v_1),(\bar{u}_1,\bar{v}_1)}$ and $D_{(u_2,v_2),(\bar{u}_2,\bar{v}_2)}$ are obtained from convolutional encoder analysis, entry of the product-state of hyper-trellis for TTCM encoders is calculated by (42). To reduce the complexity of calculating the generating function, it is assumed that j-times single error event occurring from a good state and ending a good state [45]. As a result, the probability of j-times error probability can be expressed as

$$[E_i(I)]^j = \left[\left(\mathbf{1}^T \mathbf{S}_{\mathcal{GB}}\right)^T [\mathbf{I} - \mathbf{S}_{\mathcal{BB}}]^{-1} \mathbf{S}_{\mathcal{BG}} \mathbf{1}\right]^j. \quad (45)$$

The approximated bit error probability of the TTCM encoder in the error floor region can be obtained as

$$P_b \approx \sum_{j_1}^{N}\sum_{j_2}^{N} \frac{N^{(j_1+j_2)}\,[E_i(I)]^{j_1}\,[E_i(I)]^{j_2}}{j_1! j_2!}, \quad (46)$$

where the approximation term in (46) is a result of the Stirling approximation which is used in the calculation for each convolutional encoder, as in the similar one given in [45]. We validate (46) via simulation in Section VI.

VI. Numerical Results

In this section, we present simulation results in order to validate the upper bound BER expressions and observe the their tightness over different scenarios. In all scenarios considered, it is assumed that the wireless channel coefficients remain constant during one symbol duration, and the natural bit-to-symbol mapping rule is selected to generate output symbols

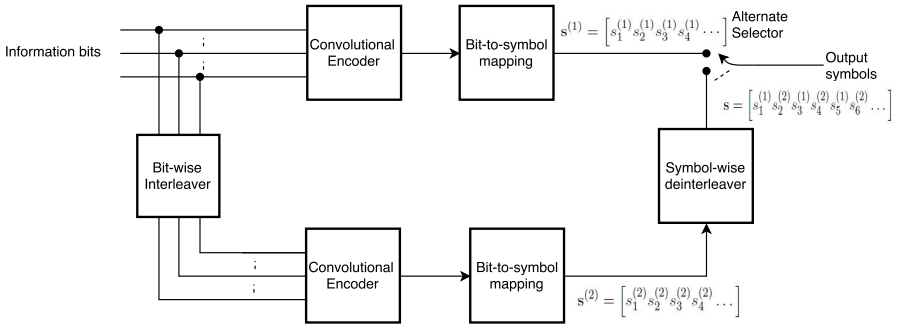

Fig. 3. Block diagram of the turbo trellis-coded modulation encoder.

from encoded bits.[2] Soft-decision Viterbi decoding is used once the ML metric is calculated from received signals from all orthogonal transmission stages. For all simulations, BER curves are plotted with respect to the average transmitted SNR per information bit, γ, in a given orthogonal stage.

Different correlation models have been proposed for a wide range of physical conditions such the exponential and one-ring model [46]. Since the analytical framework presented here is independent from how the values of ρ_{ij} are generated, it is applicable to any spatial correlation model. Due to its simplicity, the exponential correlation model is used in the simulations where ρ_{ij} follows an exponential delay such that $\rho_{ij} = r_k^{|i-j|}$ for some r_k [47], [48].

A. A Comparison of the QR and Non-QR Cases

We begin by highlighting the effects of quasi-regularity on the error bound calculation, thus demonstrating the necessity for utilizing the proposed product-state matrix method. We consider a TMRC case with a rate $R = 1/2$ convolutional encoder $[2, 1]_8$. For a quick reference for conventional generating function calculation, please see Appendix B; please refer to [9, Ch. 13] and [49, Ch. 4] for more details.

For the TMRC scenario, one QR case is considered using the regular QAM constellation, $\{1 + 1i, -1 + 1i, 1 - 1i, -1 - 1i\}$, while the non-QR scenario uses a 4-ary signal constellation, $\chi^{(1)}$, given in Table III. It is important to note that each $\chi^{(i)}$ was chosen such that it is not quasi-regular along with the $[2, 1]_8$ convolutional encoder, based on (38), within the sample set generated by a standard uniform distribution generator under an average symbol energy constraint ($i \in \{1, 2, 3\}$). For this scenario we consider a single transmission stage with two transmit antennas $\left(K = 1, N^{(1)} = 2\right)$ with channel parameters $m_1 = m_2 = 2.5$ and unit fading power. Unlike the single transmit antenna cases, the generating function calculation utilizes (19) in both conventional [9, (13.50)] and product-state matrix methods, since (19) is required for the transition probability for the TMRC system considered. It is important to note that upper bound BER curves for the conventional method are plotted based on (10) without any tightening constants as those given in [17]. Therefore, the comparison herein aims to demonstrate

[2]For instance, in a 16-ary signalling scheme, s_6 corresponds to the following 4 bits: 0110.

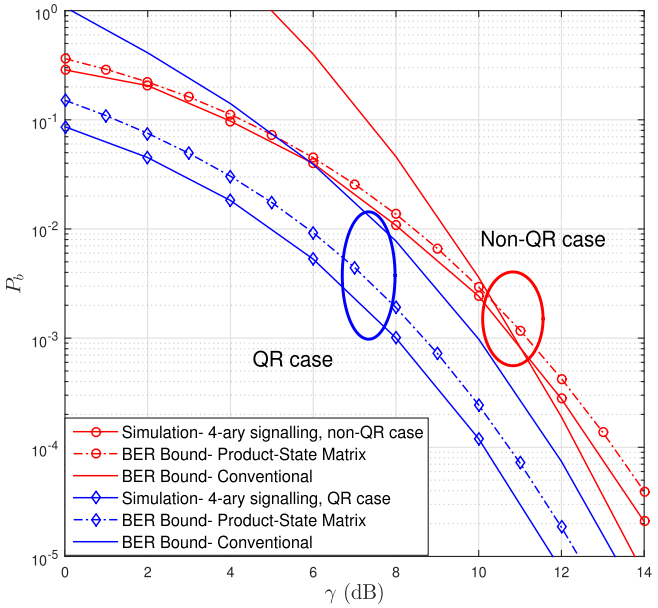

Fig. 4. Bound comparison for 4-ary signalling with the TMRC system.

that the conventional method no longer produces a valid bound in non-QR cases, rather than demonstrating which method gives the tighter bound.

In Fig. 4, the proposed BER bound expression is very tight for both QR and non-QR cases, while the method using conventional generating function is valid only for the QR case. Although both methods utilize the same transition probability of (19), only the product-state matrix technique gives the correct generating function for the non-QR case. This demonstrates that in the non-QR cases, the conventional BER bound does not represent a reliable error performance metric. This implies that the product-state matrix technique offers the important flexibility to be used independently of the constellation and encoder employed. In what follows, we evaluate the performance of the proposed technique in more detail.

B. Irregular 4-Ary Signalling

We consider four different irregular 4-ary constellation scenarios with a rate $R = 1/2$ convolutional encoder $[2, 1]_8$ for non-integer m values. The 2D irregular constellations are generated by a random number generator and are listed

TABLE III
SIMULATION SCENARIOS FOR 4-ARY SIGNALLING CASES

Scenarios	K	$N^{(k)}$	$m_{k,i}$	r_k	$\Omega_{k,i}$
I	2	$N^{(1)}=2$ $N^{(2)}=3$	$m_{1,1}=m_{1,2}=2.5$ $m_{2,1}=m_{2,2}=m_{2,3}=1.5$	$r_k=0,\ \forall k$	$\Omega_{1,1}=\Omega_{1,2}=1.0$ $\Omega_{2,1}=\Omega_{2,2}=\Omega_{2,3}=1.0$
II	3	$N^{(1)}=2$ $N^{(2)}=1$ $N^{(3)}=3$	$m_{1,1}=2.5,\ m_{1,2}=1.2$ $m_{2,1}=2.4$ $m_{3,1}=1.8,\ m_{3,2}=2.8,\ m_{3,3}=2.5$	$r_k=0,\ \forall k$	$\Omega_{1,1}=0.9, \Omega_{1,2}=0.7$ $\Omega_{2,1}=1.0$ $\Omega_{3,1}=0.8, \Omega_{3,2}=0.9, \Omega_{3,3}=1.0$
III	1	$N^{(1)}=2$	$m_{1,1}=m_{1,2}=m_{1,3}=3.2$	$r_1=0.8$	$\Omega_{1,1}=\Omega_{1,2}=\Omega_{1,3}=1.0$
IV	2	$N^{(1)}=2$ $N^{(2)}=2$	$m_{1,1}=m_{1,2}=2.4$ $m_{2,1}=1.5,\ m_{2,2}=1.8$	$r_1=0.7$ $r_2=0.0$	$\Omega_{1,1}=\Omega_{1,2}=0.8$ $\Omega_{2,1}=0.7, \Omega_{2,2}=1.0$
$\chi^{(1)}=\{-1.3295-0.5003i, -0.1550+1.8850i, -0.3707+0.8251i, -1.2487+0.1667i\}$					
$\chi^{(2)}=\{2.2094-0.8762i, -0.8014+0.7153i, -0.2460-0.0759i, -0.7526+0.7512i\}$					
$\chi^{(3)}=\{-1.9607-0.3067i, -0.7829-1.0952i, -0.5734+1.1526i, -1.0863+0.7867i\}$					

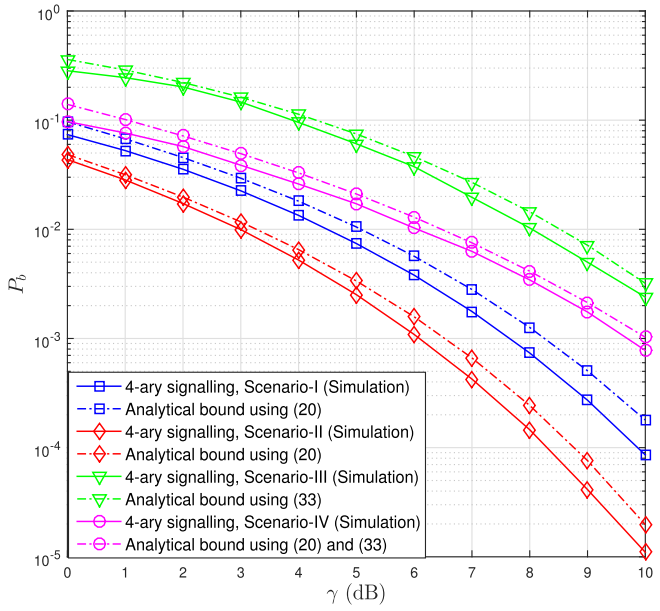

Fig. 5. Bit error probability for 4-ary signalling over different scenarios.

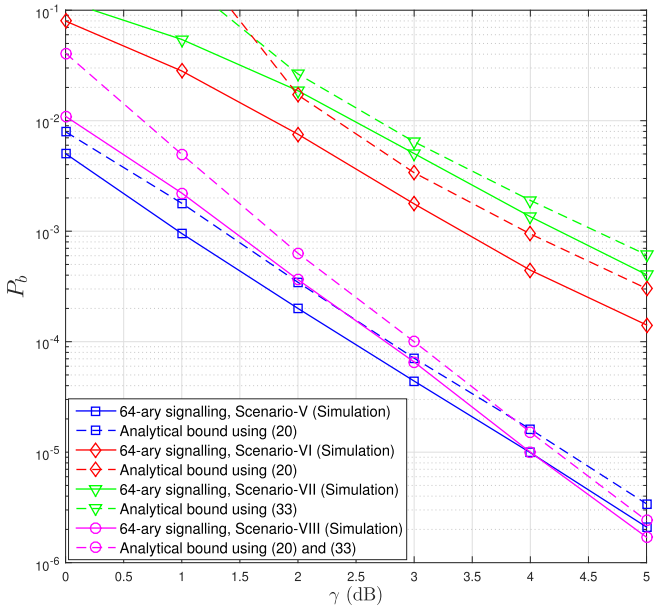

Fig. 6. Bit error probability for 64-ary signalling over different scenarios.

in Table III, along with the other simulation parameters. Uncorrelated fading is assumed in the first two scenarios, while Scenario III and Scenario IV include spatial correlation. Scenario II represents distributed antenna transmission, where the fading parameters $m_{k,i}$ and $\Omega_{k,i}$ can vary between antennas. For instance, it features 1.1 dB SNR difference between the second transmit and first transmit antennas in the 1st transmission stage. For Scenarios III and IV, the eigenvalues of the matrix of $\mathbf{A}_k$ are required for the calculation of (32). Using $\rho_{ij}=r_k^{|i-j|}$ and (28), $\mathbf{C}_k$ is first calculated based on the values of r_k given in Table II, then $\mathbf{C}_k$ is multiplied with (27), which is defined as $\mathbf{A}_k$.

In Scenario III, the eigenvalues are given by $\{\lambda_{1,i}\}_i^3 = \{0.0220,\ 0.0608,\ 0.8547\}$ and they are listed as $\{\lambda_{1,i}\}_i^2 = \{0.0523,\ 0.6144\}$ and $\{\lambda_{2,i}\}_i^2 = \{0.4667,\ 0.6667\}$ for Scenario IV. Note that in some scenarios, the correlation characteristic requires the use of (19) and (32) in the BER bound calculation. For instance, although the first orthogonal stage shows correlation between its transmit antennas, there is only one transmit antenna deployed in the second transmission stage. For the above scenarios, Fig. 5 shows the BER values generated by Monte Carlo simulations and the derived upper bound BER expressions resulting from (19) for uncorrelated and (32) for correlated cases. Fig. 5 demonstrates that the developed upper bound BER expressions yield good agreement with simulations for both uncorrelated and correlated fading cases.

C. Irregular 64-Ary Signalling

In the case of 64-ary signalling, a rate $R = 1/3$ convolutional encoder $[133, 171, 165]_8$, specified in the 3GPP LTE standard for use in downlink control information (DCI) [38], is used. Integer-valued Nakagami-m values are only considered for these scenarios for simplicity. To generate irregular 64-ary constellations, the technique given in [31], originally proposed for generating non-uniform M-ary constellations, is implemented. Specifically, conventional 64-QAM is first separated into two subsets, similar to the first step of the set partitioning process in conventional TCM design. Subsequently, one of these subsets is rotated by a specific angle θ_k for each orthogonal stage. Instead of generating 64-ary irregular constellations for all cases, 64-ary non-uniform constellations given in [7]

TABLE IV
SIMULATION SCENARIOS FOR 64-ARY SIGNALLING CASES

Scenarios	K	$N^{(k)}$	$m_{k,i}$	r_k	θ_k	$\Omega_{k,i}$
V	3	$N^{(1)}=2$ $N^{(2)}=1$ $N^{(3)}=2$	$m_{1,1}=2.0,\ m_{1,2}=1.0$ $m_{2,1}=2.0$ $m_{3,1}=3.0,\ m_{3,2}=1.0$	$r_k=0,\ \forall k$	$\theta_1=0$ $\theta_2=\pi/3$ $\theta_3=\pi/6$	$\Omega_{1,1}=1.0, \Omega_{1,2}=0.6$ $\Omega_{2,1}=1.0$ $\Omega_{3,1}=0.8, \Omega_{3,2}=1.0$
VI	2	$N^{(1)}=2$ $N^{(2)}=2$	$m_{1,1}=1.0,\ m_{1,2}=2.0$ $m_{2,1}=m_{2,2}=1.0$	$r_k=0,\ \forall k$	N/A Constellations in [7]	$\Omega_{1,1}=1.0, \Omega_{1,2}=0.8$ $\Omega_{2,1}=\Omega_{2,2}=1.0$
VII	2	$N^{(1)}=3$ $N^{(2)}=2$	$m_{1,1}=m_{1,2}=m_{1,3}=4.0$ $m_{2,1}=m_{2,2}=3.0$	$r_1=0.8$ $r_2=0.7$	N/A Constellations in [7]	$\Omega_{k,i}=1,\ \forall k,\ i$
VIII	3	$N^{(1)}=2$ $N^{(2)}=2$ $N^{(3)}=1$	$m_{1,1}=m_{1,2}=2.0$ $m_{2,1}=1.0,\ m_{2,2}=2.0$ $m_{3,1}=1.0$	$r_1=0.9$ $r_2=0.0$ $r_3=0.0$	$\theta_1=0$ $\theta_2=\pi/3$ $\theta_3=\pi/6$	$\Omega_{1,1}=0.6,\ \Omega_{1,2}=0.6$ $\Omega_{2,1}=0.8,\ \Omega_{2,2}=1.0$ $\Omega_{3,1}=1.0$

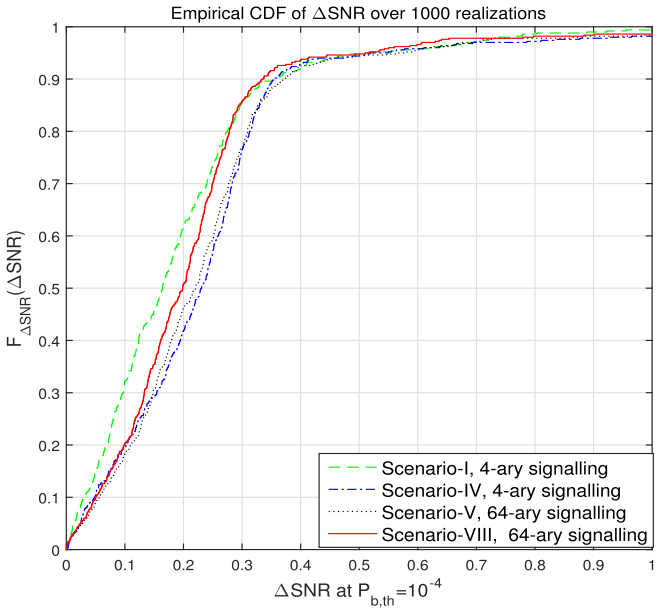

Fig. 7. The CDF of ΔSNR over 1000 irregular random constellation realizations.

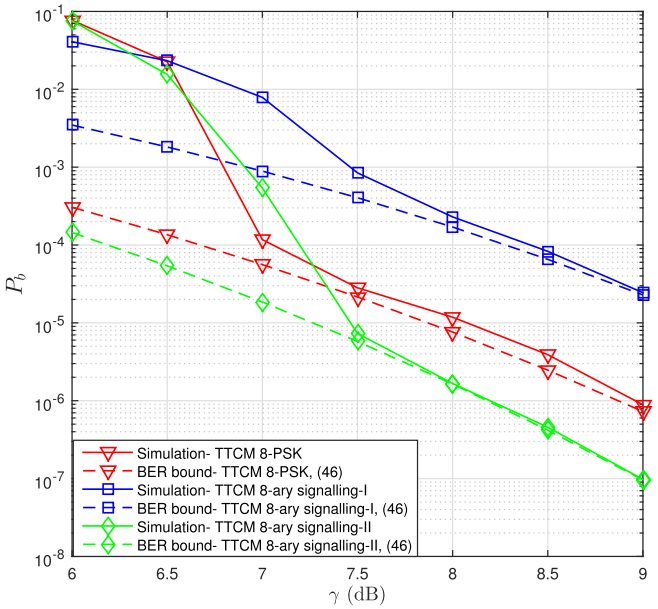

Fig. 8. Bit error probability for 8-ary signalling over different scenarios.

are also used in Scenario VI and Scenario VII. These are listed in Table IV, along with the values of the number of orthogonal stages K, Nakagami-m fading parameters $m_{k,i}$ and the number of transmitting antennas $N^{(k)}$, correlation parameter r_k, and average fading powers $\Omega_{k,i}$ for each stage.

The eigenvalues for Scenario VII are listed as $\{\lambda_{1,i}\}_i^3 = \{0.0178, 0.0489, 0.6834\}$ and $\{\lambda_{2,i}\}_i^2 = \{0.0527, 0.6140\}$, respectively. In Scenario VIII, they can be calculated as $\{\lambda_{1,i}\}_i^2 = \{0.0145, 0.5855\}$, $\{\lambda_{2,i}\}_i^2 = \{0.8000, 0.8000\}$, and $\{\lambda_{3,i}\}_i^1 = \{1.0000\}$, respectively. Fig. 6 demonstrates that the developed upper bound BER expressions yield good agreement with simulations in the moderate and high SNR regions, where P_b drops below 10^{-2}.

D. Tightness of Proposed Bound Expressions

Having presented two bound comparisons and eight different numerical scenarios, working with 4-ary and 64-ary signalling along with different types of the convolutional encoders, we have illustrated that the tightness of the upper bound curves can vary slightly within simulation parameters. Based on this observation, further investigation of the tightness of the proposed bound has become necessary to prove this tightness over a broader range of scenarios. To do so, we aim to measure the BER bound accuracy for a large number of randomly generated 4-ary and 64-ary irregular constellations, where symbol locations are determined without any assumption.

Specifically, for a BER target, $P_{b,th}$, we calculate the error ΔSNR between the actual, simulated SNR required for $P_{b,th}$, and the SNR obtained using the bound expression. By plotting the CDF of ΔSNR, the characteristics of both the uncorrelated and correlated expressions can be investigated for a broad range of irregular constellations. As seen in Fig. 7, cases in which the SNR discrepancy between the analytical and simulated cases exceeds 0.4 dB account for less than ten percent of the total generated cases. Thus, we can say that the proposed bounds perform well over most of the realizations.

E. Application to Turbo Trellis-Coded Modulation Encoder

Besides the convolutional coded cases, the bound for TTCM encoders given in (46) is validated over the AWGN channel

with a parameter set of $\left(K=1,\ N^{(1)}=1\right)$. Here, the TTCM encoder is considered [40] along with 8-ary signalling. At each constituent convolutional decoder, a symbol-by-symbol maximum a posteriori probability (MAP) decoder operates in the log domain, the information block length is chosen as 1024 and the number of turbo decoder iterations, $Q=8$. As seen in Fig. 8, the proposed analysis for the error floor region, (46), shows good agreement with simulated results for all cases. In these simulations, three different 8-ary signalling cases are considered, which are $\{1-1i, 1, 1+1i, 1i, -1+1i, -1, -1-1i, -1i\}$, $\{-1.6+0.8i, -0.6+0.8i, 0.6+0.8i, 1.6+0.8i, -1.6-0.8i, -0.6-0.8i, 0.6-0.8i, 1.6-0.8i\}$, and $\{0.28-1.1i, -0.01-0.16i, 0.13+0.82i, 1.19+0.48i, -0.80-0.59i, -1.20+0.69i, 0.98-0.54i, -0.14-0.40i\}$, respectively.

VII. Concluding Remarks

We presented the BER upper bound expressions for a generic, coded scheme which includes multiple orthogonal transmission stages and multiple transmit antennas. The proposed BER bound expressions based on the transfer function calculation from the product-state matrix are compatible with any convolutional encoder and irregular signal constellation where symbol locations can be completely arbitrary. This is in contrast to previous methods, which can only be used when the encoder and constellation satisfy the quasi-regularity condition, likely to be violated in future systems where optimized irregular constellations are used. In addition, the presented analysis is extended to the turbo trellis-coded systems to enable the irregular constellation optimization in the presence of more advanced error correcting coding techniques.

The studied coded transmit maximum ratio combining technique which has been studied here has more complexity at the transmitter side than the receiver side. This asymmetric complexity requirement may render the studied concept suitable for the downlink of the IoT applications with optimized irregular constellations

Appendix A
Solution of (23)

Beginning with (23), we first perform the change of variable $y=e^{-X_k}$, giving

$$Z_k=\int_0^1 y^{d_k-1}G_{\kappa,\kappa}^{\kappa,0}\left(y\,\middle|\,\begin{matrix}\psi_\kappa^{(1)}\\ \psi_\kappa^{(2)}\end{matrix}\right)dy. \tag{47}$$

Using [32, (9.31.5)] and the definition of the Meijer G-function [50], changing the order of the integrals allows us to write

$$\begin{aligned}Z_k&=\int_0^1 y^{d_k-1}G_{\kappa,\kappa}^{\kappa,0}\left(y\,\middle|\,\begin{matrix}\psi_\kappa^{(1)}\\ \psi_\kappa^{(2)}\end{matrix}\right)dy\\&=\frac{1}{2\pi i}\oint_C\frac{\prod_{j=1}^{\kappa}\Gamma\left(\psi_{\kappa,j}^{(2)}-s\right)}{\prod_{j=1}^{\kappa}\Gamma\left(\psi_{\kappa,j}^{(1)}-s\right)}\frac{1}{s+d_k}ds.\end{aligned} \tag{48}$$

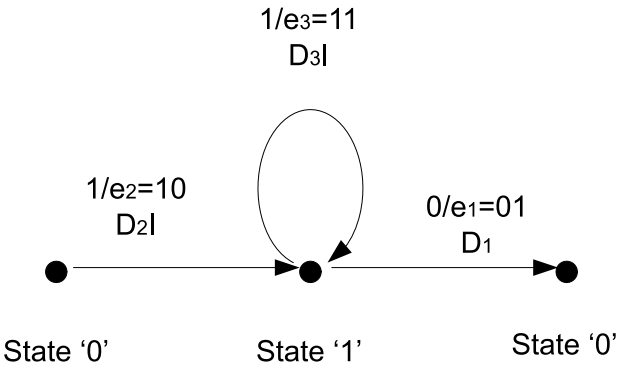

Fig. 9. Error state diagram of the $[2, 1]_8$ convolutional encoder.

Using [32, 8.331.1] in (48) gives

$$Z_k=\frac{1}{2\pi i}\oint_C\frac{1}{\prod_{i=1}^{\kappa}\left(\frac{m_{k,i}}{\Omega_{k,i}}-s\right)}\frac{1}{s+d_k}ds, \tag{49}$$

and applying Cauchy's integral formula [51],

$$f(a)=\frac{1}{2\pi i}\oint_C\frac{f(z)}{z-a}dz, \tag{50}$$

to (49), where

$$f(z)=\prod_{i=1}^{\kappa}\frac{1}{\frac{m_{k,i}}{\Omega_{k,i}}-z},\quad a=-d_k, \tag{51}$$

results in

$$Z_k=\prod_{i=1}^{\kappa}\left(d_k+\frac{m_{k,i}}{\Omega_{k,i}}\right)^{-m_{k,i}}. \tag{52}$$

This, when combined with (22), results in (24).

Appendix B
Conventional Generating Function Calculation

This appendix presents the conventional generating function calculation for a specific example. For simplicity, a rate $R=1/2$ convolutional encoder with a 4-QAM constellation is considered (see Fig. 9). Since the chosen constellation consists of four possible output symbols, e.g., $s_n\in\{s_1,s_2,s_3,s_4\}$, there are four possible pairs of the original and the erroneous symbol $(s,\hat{s})$ for the error sequence of $\{01\}$ (i.e., $n=2$). These are $\{00,01\}$, $\{01,00\}$, $\{10,11\}$, and $\{11,10\}$, assuming the natural bit-to-symbol mapping is used. The generating function is given by

$$T(I)=\frac{D_2D_1I}{1-D_3I}, \tag{53}$$

where D_n corresponds to the error weight profile for the error sequence e_n, $n\in\{1,2,3\}$. Averaging the squared distance between these possible pairs gives

$$d_2=\frac{\frac{1}{4}(|s_1-s_2|^2+|s_2-s_1|^2+|s_3-s_4|^2+|s_4-s_3|^2)}{4N_0}. \tag{54}$$

Then, $D_2(\cdot)$ is then obtained by substituting (54) into the error weight profile expression for the uncorrelated TMRC case with general m-parameters, which is

$$D_2 = \prod_{k=1}^{K}\prod_{i=1}^{N^{(k)}} - \left(\frac{m_{k,i}}{\Omega_{k,i}}\right)^{m_{k,i}} \times \bar{\mathrm{H}}^{0,N^{(k)}+1}_{N^{(k)}+1,N^{(k)}+1}\left[1 \,\middle|\, \begin{matrix}\Xi^{(1)}_{N^{(k)}}, (1+d_2, 1, 1) \\ \Xi^{(2)}_{N^{(k)}}, (d_n, 1, 1)\end{matrix}\right], \quad (55)$$

of the same form as (19). After the same steps are taken for $D_1(\cdot)$ and $D_3(\cdot)$, (53) can be obtained.

ACKNOWLEDGMENT

The authors would like to acknowledge the insightful and constructive feedback they received from the Associate Editor and the anonymous Reviewers.

REFERENCES

[1] A. Desiraju, M. Torlak, and M. Saquib, "Multiple-attempt decoding of convolutional codes over Rayleigh channels," *IEEE Trans. Veh. Technol.*, vol. 64, no. 8, pp. 3426–3439, Aug. 2015.

[2] C. Rachinger, J. B. Huber, and R. R. Müller, "Comparison of convolutional and block codes for low structural delay," *IEEE Trans. Commun.*, vol. 63, no. 12, pp. 4629–4638, Dec. 2015.

[3] A. R. Williamson, T. Y. Chen, and R. D. Wesel, "Variable-length convolutional coding for short blocklengths with decision feedback," *IEEE Trans. Commun.*, vol. 63, no. 7, pp. 2389–2403, Jul. 2015.

[4] D. Sahinel, C. Akpolat, M. A. Khan, F. Sivrikaya, and S. Albayrak, "Beyond 5G vision for IOLITE community," *IEEE Commun. Mag.*, vol. 55, no. 1, pp. 41–47, Jan. 2017.

[5] M. T. Malik, M. J. Hossain, and M.-S. Alouini, "Generalized BICM-T transceivers: Constellation and multiplexer design," in *Proc. IEEE 24th Int. Symp. Pers. Indoor Mobile Radio Commun. (PIMRC)*, Sep. 2013, pp. 466–470.

[6] J. Zöllner and N. Loghin, "Optimization of high-order non-uniform QAM constellations," in *Proc. IEEE Int. Symp. Broadband Multimedia Syst. Broadcast. (BMSB)*, Jun. 2013, pp. 1–6.

[7] A. B. Sediq, P. Djukic, H. Yanikomeroglu, and J. Zhang, "Optimized nonuniform constellation rearrangement for cooperative relaying," *IEEE Trans. Veh. Technol.*, vol. 60, no. 5, pp. 2340–2347, Jun. 2011.

[8] G. C. Alexandropoulos, N. C. Sagias, F. I. Lazarakis, and K. Berberidis, "New results for the multivariate Nakagami-*m* fading model with arbitrary correlation matrix and applications," *IEEE Trans. Wireless Commun.*, vol. 8, no. 1, pp. 245–255, Jan. 2009.

[9] M. K. Simon and M.-S. Alouini, *Digital Communication Over Fading Channels*. Hoboken, NJ, USA: Wiley, 2005.

[10] D. Divsalar and M. K. Simon, "The design of trellis coded MPSK for fading channels: Performance criteria," *IEEE Trans. Commun.*, vol. COM-36, no. 9, pp. 1004–1012, Sep. 1988.

[11] L. Hanzo, S. X. Ng, W. Webb, and T. Keller, *Quadrature Amplitude Modulation: From Basics to Adaptive Trellis-Coded, Turbo-Equalised and Space-Time Coded OFDM, CDMA and MC-CDMA Systems*. Hoboken, NJ, USA: Wiley, 2004.

[12] A. Maaref and S. Aïssa, "Exact error probability analysis of rectangular QAM for single- and multichannel reception in Nakagami-*m* fading channels," *IEEE Trans. Commun.*, vol. 57, no. 1, pp. 214–221, Jan. 2009.

[13] P. G. Moschopoulos, "The distribution of the sum of independent gamma random variables," *Ann. Inst. Statist. Math.*, vol. 37, no. 1, pp. 541–544, 1985.

[14] G. K. Karagiannidis, N. C. Sagias, and T. A. Tsiftsis, "Closed-form statistics for the sum of squared Nakagami-*m* variates and its applications," *IEEE Trans. Commun.*, vol. 54, no. 8, pp. 1353–1359, Aug. 2006.

[15] I. S. Ansari, F. Yilmaz, M.-S. Alouini, and O. Kucur, "New results on the sum of Gamma random variates with application to the performance of wireless communication systems over Nakagami-*m* fading channels," *Trans. Emerg. Telecommun. Technol.*, vol. 28, no. 1, p. e2912, 2017. [Online]. Available: http://dx.doi.org/10.1002/ett.2912

[16] S. A. Al-Semari and T. E. Fuja, "Performance analysis of coherent TCM systems with diversity reception in slow Rayleigh fading," *IEEE Trans. Veh. Technol.*, vol. 48, no. 1, pp. 198–212, Jan. 1999.

[17] S. A. Zummo, "Union bounds on the bit error probability of coded MRC in Nakagami-*m* fading," *IEEE Commun. Lett.*, vol. 10, no. 11, pp. 769–771, Nov. 2006.

[18] S. Benedetto, M. Mondin, and G. Montorsi, "Performance evaluation of trellis-coded modulation schemes," *Proc. IEEE*, vol. 82, no. 6, pp. 833–855, Jun. 1994.

[19] S. Nagaraj, "Performance analysis of coded SSK modulation on block-fading channels," *IEEE Trans. Veh. Technol.*, vol. 65, no. 8, 6773–6777, Aug. 2016, doi: 10.1109/TVT.2015.2477295.

[20] R. D. Wesel, "Reduced-state representations for trellis codes using constellation symmetry," *IEEE Trans. Commun.*, vol. 52, no. 8, pp. 1302–1310, Aug. 2004.

[21] J.-E. Porath and T. Aulin, "Design of multidimensional signal constellations," *IEE Proc.-Commun.*, vol. 150, no. 5, pp. 317–323, Oct. 2003.

[22] F. Kayhan and G. Montorsi, "Constellation design for channels affected by phase noise," in *Proc. IEEE Int. Conf. Commun. (ICC)*, Jun. 2013, pp. 3154–3158.

[23] C. Häger, A. Graell i Amat, A. Alvarado, and E. Agrell, "Design of APSK constellations for coherent optical channels with nonlinear phase noise," *IEEE Trans. Commun.*, vol. 61, no. 8, pp. 3362–3373, Aug. 2013.

[24] M. C. Ilter, H. Yanikomeroglu, and P. A. Dmochowski, "BER upper bound expressions in coded two-transmission schemes with arbitrarily spaced signal constellations," *IEEE Commun. Lett.*, vol. 20, no. 2, pp. 248–251, Feb. 2016.

[25] E. Biglieri, "High-level modulation and coding for nonlinear satellite channels," *IEEE Trans. Commun.*, vol. COM-32, no. 5, pp. 616–626, May 1984.

[26] T. K. Y. Lo, "Maximum ratio transmission," *IEEE Trans. Commun.*, vol. 47, no. 10, pp. 1458–1461, Oct. 1999.

[27] P. A. Dighe, R. K. Mallik, and S. S. Jamuar, "Analysis of transmit-receive diversity in Rayleigh fading," *IEEE Trans. Commun.*, vol. 51, no. 4, pp. 694–703, Apr. 2003.

[28] O. Bello and S. Zeadally, "Intelligent device-to-device communication in the Internet of Things," *IEEE Syst. J.*, vol. 10, no. 3, pp. 1172–1182, Sep. 2016.

[29] M. C. Ilter and H. Yanikomeroglu, "An upper bound on BER in a coded two-transmission scheme with same-size arbitrary 2D constellations," in *Proc. IEEE Int. Symp. Pers., Indoor Mobile Radio Commun. (PIMRC)*, Washington, DC, USA, Sep. 2014, pp. 687–691.

[30] J. Shi and R. D. Wesel, "Efficient computation of trellis code generating functions," *IEEE Trans. Commun.*, vol. 52, no. 2, pp. 219–227, Feb. 2004.

[31] D. Divsalar, M. Simon, and J. Yuen, "Trellis coding with asymmetric modulations," *IEEE Trans. Commun.*, vol. COM-35, no. 2, pp. 130–141, Feb. 1987.

[32] I. S. Gradshteyn and I. Ryzhik, *Table of Integrals, Series, and Products*, 7th ed. New York, NY, USA: Academic, 2007.

[33] I. S. Ansari, F. Yilmaz, M.-S. Alouini, and O. Kucur, "On the sum of gamma random variates with application to the performance of maximal ratio combining over Nakagami-*m* fading channels," in *Proc. IEEE Int. Workshop Signal Process. Adv. Wireless Commun. (SPAWC)*, Cesme, Turkey, Jun. 2012, pp. 394–398.

[34] M. S. Alouini, A. Abdi, and M. Kaveh, "Sum of gamma variates and performance of wireless communication systems over Nakagami-fading channels," *IEEE Trans. Veh. Technol.*, vol. 50, no. 6, pp. 1471–1480, Nov. 2001.

[35] Q. T. Zhang, "A decomposition technique for efficient generation of correlated Nakagami fading channels," *IEEE J. Sel. Areas Commun.*, vol. 18, no. 11, pp. 2385–2392, Nov. 2000.

[36] Z. Shi, S. Ma, and K.-W. Tam, "Rate selection for cooperative HARQ-CC systems over time-correlated Nakagami-*m* fading channels," in *Proc. IEEE Int. Conf. Commun. Workshop (ICCW)*, London, U.K., Jun. 2015, pp. 919–924.

[37] R. D. Wesel, "Reduced complexity trellis code transfer function computation," in *Proc. Commun. Theory Mini-Conf.*, Jun. 1999, pp. 37–41.

[38] *Evolved Universal Terrestrial Radio Access (E-UTRA); Multiplexing and Channel Coding*, document 3GPP TS 36.212 Version 8.7. 0 Release 8, Jun. 2009.

[39] C. Berrou, A. Glavieux, and P. Thitimajshima, "Near Shannon limit error-correcting coding and decoding: Turbo-codes. 1," in *Proc. IEEE Int. Conf. Commun. (ICC)*, vol. 2. May 1993, pp. 1064–1070.

[40] P. Robertson and T. Wörz, "Bandwidth-efficient turbo trellis-coded modulation using punctured component codes," *IEEE J. Sel. Areas Commun.*, vol. 16, no. 2, pp. 206–218, Feb. 1998.

[41] S. X. Ng, O. R. Alamri, Y. Li, J. Kliewer, and L. Hanzo, "Near-capacity turbo trellis coded modulation design based on EXIT charts and union bounds," *IEEE Trans. Commun.*, vol. 56, no. 12, pp. 2030–2039, Dec. 2008.
[42] O. Y. Takeshita, O. M. Collins, P. C. Massey, and D. J. Costello, "A note on asymmetric turbo-codes," *IEEE Commun. Lett.*, vol. 3, no. 3, pp. 69–71, Mar. 1999.
[43] S. Benedetto and G. Montorsi, "Unveiling turbo codes: Some results on parallel concatenated coding schemes," *IEEE Trans. Inf. Theory*, vol. 42, no. 2, pp. 409–428, Mar. 1996.
[44] H. Ogiwara, A. Mizutome, and K. Koike, "Performance evaluation of parallel concatenated trellis-coded modulation," *IEICE Trans. Fundam. Electron., Commun. Comput. Sci.*, vol. E84-A, no. 10, pp. 2410–2417, 2001.
[45] M. Griot, A. I. V. Casado, and R. Wesel, "Nonlinear turbo codes for higher-order modulations," in *Proc. IEEE Int. Conf. Commun. (ICC)*, Beijing, China, May 2008, pp. 1209–1213.
[46] A. Forenza, D. J. Love, and R. W. Heath, Jr., "Simplified spatial correlation models for clustered MIMO channels with different array configurations," *IEEE Trans. Veh. Technol.*, vol. 56, no. 4, pp. 1924–1934, Jul. 2007.
[47] S. L. Loyka, "Channel capacity of MIMO architecture using the exponential correlation matrix," *IEEE Commun. Lett.*, vol. 5, no. 9, pp. 369–371, Sep. 2001.
[48] C. Oestges, "Validity of the Kronecker model for MIMO correlated channels," in *Proc. IEEE Veh. Technol. Conf. (VTC-Spring)*, Melbourne, VIC, Australia, May 2006, pp. 2818–2822.
[49] A. J. Viterbi and J. K. Omura, *Principles of Digital Communication and Coding*. New York, NY, USA: McGraw-Hill, 1979.
[50] L. L. Yang and H. H. Chen, "Error probability of digital communications using relay diversity over Nakagami-*m* fading channels," *IEEE Trans. Wireless Commun.*, vol. 7, no. 5, pp. 1806–1811, May 2008.
[51] F. B. Hildebrand, *Advanced Calculus for Applications*. Englewood Cliffs, NJ, USA: Prentice-Hall, 1962.

Mehmet Cagri Ilter (S'11) received the B.Sc. degree in telecommunication engineering and the M.A.Sc. degree in electronics and communication engineering from Istanbul Technical University, Istanbul, Turkey, in 2009 and 2013, respectively. He is currently pursuing the Ph.D. degree in electrical and computer engineering from Carleton University, Ottawa, ON, Canada, and is a member of the 5G research project with Huawei Technologies. His research interests include 5G networks, constellation and encoder design, error correcting codes, network coding, network coded cooperation, signal space diversity, applied probability, and applications of optimization in wireless networks.

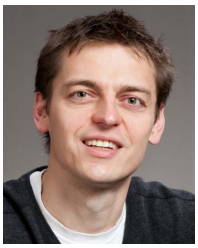

Pawel A. Dmochowski (S'02–M'07–SM'11) was born in Gdansk, Poland. He received the B.A.Sc. in engineering physics from the University of British Columbia in 1998, and the M.Sc. and Ph.D. degrees from Queen's University, Kingston, Ontario, in 2001 and 2006, respectively. He was a Natural Sciences and Engineering Research Council Visiting Fellow with the Communications Research Centre Canada. He is currently a Senior Lecturer with the School of Engineering and Computer Science, Victoria University of Wellington, New Zealand. From 2014 to 2015, he was a Visiting Professor with Carleton University, Ottawa. From 2014 to 2015, he was the Chair of the IEEE Vehicular Technology Society Chapters Committee. He currently serves as an Editor for IEEE COMMUNICATIONS LETTERS and the IEEE WIRELESS COMMUNICATIONS LETTERS. His research interests include mmWave, massive mimo, and cognitive radio systems.

Halim Yanikomeroglu (F'17) was born in Giresun, Turkey, in 1968. He received the B.Sc. degree in electrical and electronics engineering from the Middle East Technical University, Ankara, Turkey, and the M.A.Sc. degree in electrical engineering (now ECE) and the Ph.D. degree in electrical and computer engineering from the University of Toronto, Toronto, ON, Canada, in 1990, 1992, and 1998, respectively. From 1993 to 1994, he was with the Research and Development Group of Marconi Kominikasyon A.S., Ankara, Turkey. Since 1998, he has been with the Department of Systems and Computer Engineering, Carleton University, Ottawa, ON, Canada, where he is currently a Full Professor. From 2011 to 2012, he spent the academic year at TOBB University of Economics and Technology, Ankara, as a Visiting Professor. His research interests include wireless technologies with a special emphasis on wireless networks. In recent years, his research has been funded by Huawei, Telus, Allen Vanguard, Mapsted, Blackberry, Samsung, Communications Research Centre of Canada, and DragonWave. This collaborative research resulted in over 30 patents (granted and applied). He is a Registered Professional Engineer in Ontario, Canada. He has been involved in the organization of the IEEE Wireless Communications and Networking Conference (WCNC) from its inception, including serving as a Steering Committee and the Technical Program Chair or Co-Chair of WCNC 2004 (Atlanta, GA, USA), WCNC 2008 (Las Vegas, NV, USA), and WCNC 2014 (Istanbul, Turkey). He was the General Co-Chair of the IEEE Vehicular Technology Conference (VTC) 2010-Fall held in Ottawa, and the General Chair of IEEE VTC 2017-Fall held in Toronto. He has served on the Editorial Boards of the IEEE TRANSACTIONS ON COMMUNICATIONS, the IEEE TRANSACTIONS ON WIRELESS COMMUNICATIONS, and THE IEEE COMMUNICATIONS SURVEYS AND TUTORIALS. He was the Chair of the IEEE Technical Committee on Personal Communications (now called Wireless Technical Committee). He is a Fellow of the IEEE, a Distinguished Lecturer for the IEEE Communications Society and a Distinguished Speaker for the IEEE Vehicular Technology Society. He was the recipient of the IEEE Ottawa Section Outstanding Educator Award in 2014, Carleton University Faculty Graduate Mentoring Award in 2010, the Carleton University Graduate Students Association Excellence Award in Graduate Teaching in 2010, and the Carleton University Research Achievement Award in 2009.